STRUCTURAL CHEMISTRY

ISSN 2053-2296

Formation of a diiron–(μ-η^1:η^1-CN) complex from acetonitrile solution

Tim P. Schlachta, Michael J. Sauer, Leon F. Richter and Fritz E. Kühn*

Technical University of Munich, School of Natural Sciences, Department of Chemistry and Catalysis Research Center, Molecular Catalysis, Lichtenbergstrasse 4, 85748 Garching, Germany. *Correspondence e-mail: fritz.kuehn@ch.tum.de

Received 11 June 2024
Accepted 18 July 2024

Edited by D. R. Turner, University of Monash, Australia

Keywords: organometallic iron(II) complex; acetonitrile cleavage; N-heterocyclic carbene; NHC; crystal structure; cyanation.

CCDC reference: 2326821

Supporting information: this article has supporting information at journals.iucr.org/c

The activation of C—C bonds by transition-metal complexes is of continuing interest and acetonitrile (MeCN) has attracted attention as a cyanide source with comparatively low toxicity for organic cyanation reactions. A diiron end-on μ-η^1:η^1-CN-bridged complex was obtained from a crystallization experiment of an open-chain iron–NHC complex, namely, μ-cyanido-κ^2C:N-bis{[(acetonitrile-κN)[3,3′-bis(pyridin-2-yl)-1,1′-(methylidene)bis(benzimidazol-2-ylidene)]iron(II)} tris(hexafluorophosphate), $[Fe_2(CN)(C_2H_3N)_2(C_{25}H_{18}N_6)_2](PF_6)_3$. The cyanide appears to originate from the MeCN solvent by C—C bond cleavage or through carbon–hydrogen oxidation.

1. Introduction

The first iron–NHC (N-heterocyclic carbene) complex was developed by Öfele in 1969 (Öfele, 1969). However, it has taken many years for iron–NHC complexes to attract the attention of a wider audience of chemists, but, especially in the last decade, there has been a sharp increase in related publications (Riener *et al.*, 2014). The open-chain iron–pyridine-NHC complex bis(acetonitrile-κN)[3,3′-bis(pyridin-2-yl)-1,1′-(methylidene)bis(benzimidazol-2-ylidene)]iron(II) bis(hexafluorophosphate), **1** (Scheme 1), can be successfully employed in homogeneous epoxidation catalysis (Schlachta *et al.*, 2024). In the present work, a diiron end-on μ-η^1:η^1-CN-bridged complex, **2** (Scheme 2), is formed from a solution of **1** in deuterated acetonitrile. The activation of C—C bonds by transition-metal complexes is of continuing interest and MeCN has attracted attention as a cyanide source with comparatively low toxicity for organic cyanation reactions (Ahmad *et al.*, 2020; Lu *et al.*, 2004; Spentzos *et al.*, 2020; Grirrane *et al.*, 2016).

2. Experimental

2.1. General procedures and analytical methods

Complex **1** was synthesized according to a literature method (Schlachta *et al.*, 2024). Solvents were purified, dried and degassed using standard methods (Armarego, 2017) or received from a solvent purification system by M. Braun. All other chemicals were obtained from commercial suppliers and were used without further purification. NMR spectra were recorded on a Bruker Avance Ultrashield AV400 (400.13 MHz for ^{1}H NMR and 100.53 MHz for ^{13}C NMR). The chemical shifts are given in δ values in ppm (parts per million) relative to TMS (tetramethylsilane) and are reported relative to the residual deuterated solvent signal (Fulmer *et al.*, 2010). Electrospray ionization mass spectrometry (ESI–MS) data were measured

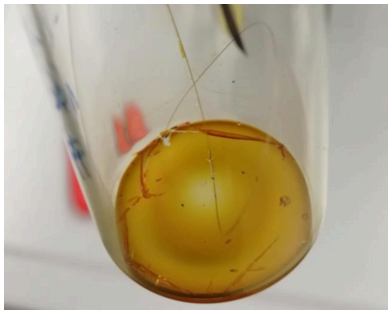

on a Thermo Fisher Ultimate 3000. FT–IR measurements were conducted on a PerkinElmer Frontier FT–IR spectrometer (ATR). The 'inVia Reflex Raman System' comprises a research grade optical microscope [Leica DM2700M, Magnification 5×, 20× and 50× (in this case, 50× was used)] coupled to a high-performance Raman spectrometer (Renishaw). A 633 nm wavelength laser was used (Renishaw RL633 Class 3B).

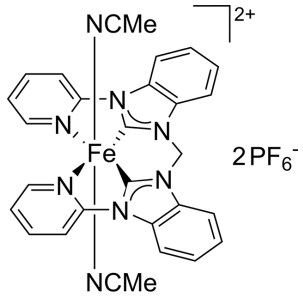

1

Scheme 1

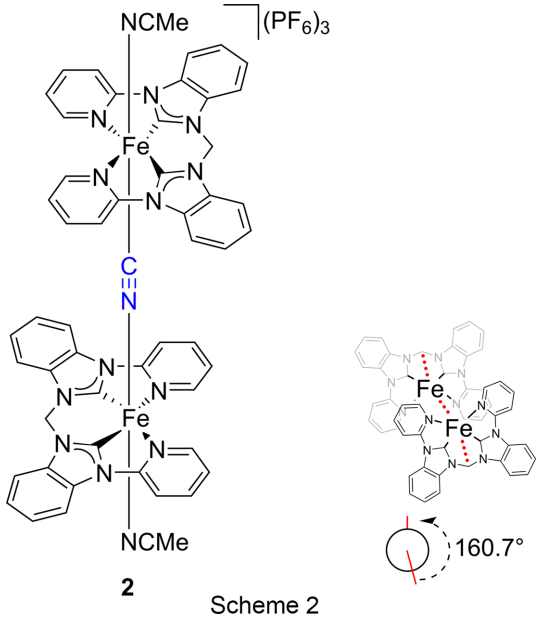

2

Scheme 2

2.2. Crystallization of 2

Single crystals of **2** suitable for X-ray diffraction were obtained by slow evaporation of a solution of **1** in CD_3CN over a period of six months at room temperature under an ambient atmosphere near a window with sunlight (see supporting information).

A solution of **1** (around 1–2 mg) in CD_3CN (around 0.4 ml, dry and degassed) from an NMR tube (see supporting information) was placed in a 10 ml vial under an ambient atmosphere. A human hair was fixed with adhesive tape to the inside of the vial, reaching into the solution. Heterogeneous nucleation occurs more frequently than homogeneous nucleation (Sear, 2014; Pruppacher & Klett, 1997) and human hair has been used for the growth of nanoparticles or as catalyst-support material (Deng *et al.*, 2016; Liu *et al.*, 2015; Haveli *et al.*, 2012; Walter *et al.*, 2006). The vial was closed and the cap was punctured with a cannula. The vial was left for six months at room temperature under ambient conditions near a window with sunlight, allowing the solvent to evaporate slowly. Orange crystals suitable for SC-XRD analysis were obtained.

Table 1
Experimental details.

Crystal data	
Chemical formula	$[Fe_2(CN)(C_2D_3N)_2(C_{25}H_{18}N_6)_2](PF_6)_3$
M_r	1465.67
Crystal system, space group	Monoclinic, *C*2/*c*
Temperature (K)	100
a, *b*, *c* (Å)	25.562 (2), 17.0373 (15), 14.8998 (12)
β (°)	112.112 (3)
V (Å^3)	6011.8 (9)
Z	4
Radiation type	Mo $K\alpha$
μ (mm^{-1})	0.67
Crystal size (mm)	0.13 × 0.05 × 0.04
Data collection	
Diffractometer	Bruker D8 Venture
Absorption correction	Multi-scan (*SADABS*; Bruker, 2016)
T_{min}, T_{max}	0.708, 0.745
No. of measured, independent and observed [$I > 2\sigma(I)$] reflections	89835, 5310, 4621
R_{int}	0.051
(sin $\theta/\lambda)_{max}$ (Å^{-1})	0.595
Refinement	
$R[F^2 > 2\sigma(F^2)]$, $wR(F^2)$, S	0.031, 0.083, 1.11
No. of reflections	5310
No. of parameters	461
No. of restraints	9
H-atom treatment	H-atom parameters constrained
$\Delta\rho_{max}$, $\Delta\rho_{min}$ (e Å^{-3})	0.43, −0.27

Computer programs: *APEX4* (Bruker, 2021), *SAINT* (Bruker, 2019), *SHELXT* (Sheldrick, 2015*a*), *SHELXL2019* (Sheldrick, 2015*b*), *PLATON* (Spek, 2020) and *enCIFer* (Allen *et al.*, 2004).

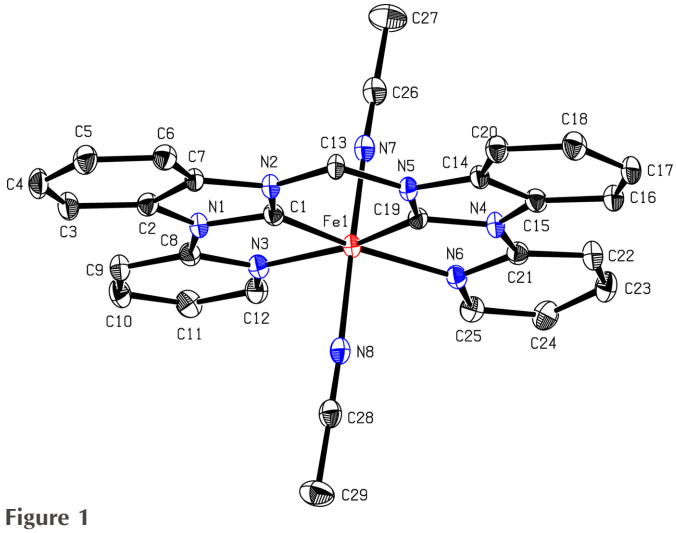

Figure 1
The molecular structure of **1**. H atoms and hexafluorophosphate anions have been omitted for clarity. Displacement ellipsoids are shown at the 50% probability level (Schlachta *et al.*, 2024).

2.3. Refinement

Crystal data, data collection and structure refinement details are summarized in Table 1. H atoms could not be located in difference Fourier maps and were calculated in ideal positions (riding model), with C—H = 0.98 Å and U_{iso}(H) = 1.5U_{eq}(C) for CH_3 groups, C—H = 0.99 Å and U_{iso}(H) = 1.2U_{eq}(C) for CH_2 groups, and C—H = 0.95 Å and U_{iso}(H) = 1.2U_{eq}(C) for CH groups. Split-layer position refinement was used for atoms P2, F7, F8, F9, F10, F11 and F12 (PF_6^- anion), as well as N8 and C28 (bridging cyanide). Restraints were applied to atoms N8 and C28 to ensure reasonable ellipsoids. CD_3 has been modelled as CH_3 as there is no appreciable difference in SC-XRD.

3. Results and discussion

When a solution of **1** (Scheme 1 and Fig. 1) in CD_3CN was evaporated slowly over a period of six months under ambient conditions, a diiron end-on μ-η^1:η^1-CN-bridged complex, [(MeCN)(NHC)Fe]$_2$(μ-η^1:η^1-CN)$(PF_6)_3$ (**2**) (Scheme 2 and Fig. 2), was obtained, as determined by X-ray diffraction. The two iron centres are bridged by a cyanide anion, hence three PF_6^- anions are present in the crystal structure. Under similar conditions, *i.e.* MeCN solution, room temperature and air, a dinuclear Cu^{II} cryptate has been found to form a μ-η^1:η^1-CN-bridged complex by C—C bond cleavage of MeCN (Lu *et al.*, 2004). A possible mechanism involving the activation of the *sp*-hybridized C atom of MeCN, bound to one Cu atom (MeCN—Cu), by the second Cu centre has been suggested. The increased electrophilicity of the methyl group would allow cleavage by H_2O to form MeOH and the cyanide-bridged compound (Lu *et al.*, 2004; Ahmad *et al.*, 2020). Another possible mechanism for the formation of **2** might be the carbon–hydrogen oxidation of MeCN by iron complex **1** to form glycolonitrile, as observed previously for an iron(III) tetracarbene complex, and subsequent release of cyanide upon decay of glycolonitrile (Knapp *et al.*, 2012; Dyckhoff *et al.*, 2021; Lewis, 2008). Due to the stronger Me—CN bond (122 kcal mol^{-1}) compared to the H—CH_2CN bond (93 kcal mol^{-1}) (Spentzos *et al.*, 2020; Blanksby & Ellison, 2003; Goebbert *et al.*, 2010; Miscione & Bottoni, 2014), the carbon–hydrogen oxidation of MeCN seems to be more likely the origin of cyanide in this case. However, C—C bond cleavage of MeCN by UV irradiation is known (Grirrane *et al.*, 2016) and, given the fact that the crystallization setup with **1** was also accessible for sunlight during the extensive period of six months, C—C bond cleavage of MeCN cannot be excluded.

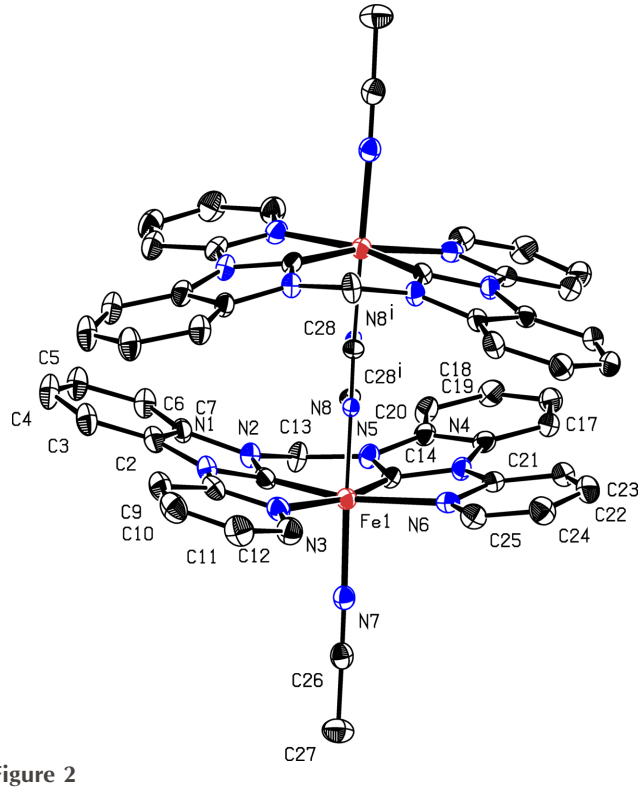

Figure 2
The molecular structure of **2**. H atoms and hexafluorophosphate anions have been omitted for clarity. Displacement ellipsoids are shown at the 50% probability level.

Table 2
Selected geometric parameters (Å, °).

Fe1—N3	2.0703 (16)	Fe1—N8	1.83 (4)
Fe1—N6	2.0754 (17)	Fe1—C1	1.824 (2)
Fe1—N7	1.9336 (17)	Fe1—C14	1.824 (2)
Fe1—C28^i	1.98 (5)	N8—C28	1.128 (12)
N7—Fe1—N8	173.3 (10)	Fe1—N8—C28	171.1 (7)
Fe1^i—C28—N8	177 (4)	N3—Fe1—C14	167.26 (8)

Symmetry code: (i) $-x+1, y, -z+\frac{1}{2}$.

The crystal structure of **2** reveals strongly bent equatorial NHC ligands. This finding is in stark contrast to **1**, where the NHC ligand is largely planar (Fig. 1). This sandwich-like structure encapsulates the cyanide ion and is indicative of some noncovalent interactions between the equatorial ligands, likely contributing to the stability of **2**. Interestingly, the pyridine units are bent less towards the centre compared to the NHC units, forming a Z-shape or diamond-shape, depending on the viewing angle of **2**. The Fe—N—C angle is slightly bent (Table 2) in a *trans* fashion, resulting in a 'zigzag' vertical axis. Another interesting finding is the rotation of the NHC ligands towards each other in an *anti* conformation, resulting in a dihedral angle (CH_2—Fe—Fe—CH_2) of 160.7° (Scheme 2). The crystal structure can in principle also be solved as the diiron–(μ-η^1:η^1-N_2) complex (Fig. 2), which is why we refrain from a detailed structural discussion at this point. However, there are several arguments against a diiron–(μ-η^1:η^1-N_2) complex:

(i) The main argument against a diiron–(μ-η^1:η^1-N_2) complex is the fact that the crystal structure contains three counter-ions. As the crystallization was performed with **1** containing an iron(II) centre, bridging two Fe^{II} atoms with a neutral N_2 ligand should lead to the presence of four counter-ions. Otherwise, three counter-ions would indicate that a redox process has occurred during the formation of **2**, but the nature of a hypothetical reducing agent and the location of reduction are highly speculative. The main components of the

crystallization experiment were **1** and CD_3CN, as well as unreacted ligand precursor as a minor impurity (see supporting information). In a cyclic voltammetry study of **1**, the first reduction event occurred at −1.78 V (*versus* Fc/Fc^+). A preliminary experiment measuring **1** in cyclic voltammetry under an N_2 atmosphere did not show significant redox processes or electric current. Considering all these facts, the involvement of a redox process appears to be quite implausible.

(ii) Dinitrogen is a weak σ-donor and a weak π-acceptor, and substitution of the N_2 ligand with CO or nitriles like MeCN is often observed (Crossland & Tyler, 2010; Sunada *et al.*, 2013). A diiron–(μ-η^1:η^1-N_2) version of **2** would be very surprising in this context, since one axial MeCN ligand coordinates with one iron centre each, the crystallization of **2** occurred in (deuterated) MeCN as solvent and the previous occupation of both axial coordination sites by MeCN in **1**. The stability of **2** under air is also interesting, which would be rather uncommon for a diiron–(μ-η^1:η^1-N_2) complex (Crossland & Tyler, 2010; Takeshita *et al.*, 2018; Saouma *et al.*, 2011; Regenauer *et al.*, 2022) and an affinity for N_2 over O_2 would be very unusual considering other Fe compounds tending to form diiron–μ-oxido species (Schlachta & Kühn, 2023; Schlachta *et al.*, 2021).

(iii) A diiron–(μ-η^1:η^1-N_2) complex should show a distinctive ν_{NN} absorption band in Raman spectroscopy and be IR inactive due to the centrosymmetric structure (Suess & Peters, 2013; McWilliams *et al.*, 2018; Gu *et al.*, 2018). No ν_{NN} band was detected in the crude material either by IR or Raman spectroscopy. However, no pronounced ν_{CN} stretch could be observed either and, interestingly, complex **1** also does not show a characteristic ν_{CN} band in IR, contrary to similar complexes (Raba *et al.*, 2012), but signals attributable to axial MeCN are visible in the Raman spectrum (see supporting information).

4. Conclusion

A diiron end-on μ-η^1:η^1-CN-bridged complex, **2**, was obtained from a crystallization experiment with an open-chain iron NHC complex **1**. The cyanide presumably originates from the MeCN solvent by C—C bond cleavage or through carbon–hydrogen oxidation. The strongly bent NHC ligands are positioned in an *anti* conformation.

Acknowledgements

Lena Schröck is gratefully acknowledged for Raman measurements. There are no competing interests to declare. Open access funding enabled and organized by Projekt DEAL.

References

Ahmad, M. S., Pulidindi, I. N. & Li, C. (2020). *New J. Chem.* **44**, 17177–17197.
Allen, F. H., Johnson, O., Shields, G. P., Smith, B. R. & Towler, M. (2004). *J. Appl. Cryst.* **37**, 335–338.
Armarego, W. L. (2017). In *Purification of laboratory chemicals*. London: Butterworth–Heinemann.
Blanksby, S. J. & Ellison, G. B. (2003). *Acc. Chem. Res.* **36**, 255–263.
Bruker (2016). *SADABS*. Bruker AXS Inc., Madison, Wisconsin, USA.
Bruker (2019). *SAINT*. Bruker AXS Inc., Madison, Wisconsin, USA.
Bruker (2021). *APEX4*. Bruker AXS Inc., Madison, Wisconsin, USA.
Crossland, J. L. & Tyler, D. R. (2010). *Coord. Chem. Rev.* **254**, 1883–1894.
Deng, D., Gopiraman, M., Kim, S. H., Chung, I.-M. & Kim, I. S. (2016). *ACS Sustainable Chem. Eng.* **4**, 5409–5414.
Dyckhoff, F., Schlagintweit, J. F., Bernd, M. A., Jakob, C. H. G., Schlachta, T. P., Hofmann, B. J., Reich, R. M. & Kühn, F. E. (2021). *Catal. Sci. Technol.* **11**, 795–799.
Fulmer, G. R., Miller, A. J. M., Sherden, N. H., Gottlieb, H. E., Nudelman, A., Stoltz, B. M., Bercaw, J. E. & Goldberg, K. I. (2010). *Organometallics*, **29**, 2176–2179.
Goebbert, D. J., Velarde, L., Khuseynov, D. & Sanov, A. (2010). *J. Phys. Chem. Lett.* **1**, 792–795.
Grirrane, A., Álvarez, E., Albero, J., García, H. & Corma, A. (2016). *Dalton Trans.* **45**, 5444–5450.
Gu, N. X., Oyala, P. H. & Peters, J. C. (2018). *J. Am. Chem. Soc.* **140**, 6374–6382.
Haveli, S. D., Walter, P., Patriarche, G., Ayache, J., Castaing, J., Van Elslande, E., Tsoucaris, G., Wang, P.-A. & Kagan, H. B. (2012). *Nano Lett.* **12**, 6212–6217.
Knapp, S. M. M., Sherbow, T. J., Juliette, J. J. & Tyler, D. R. (2012). *Organometallics*, **31**, 2941–2944.
Lewis, R. J. Sr (2008). In *Hazardous Chemicals Desk Reference*, 6th ed. Chichester: John Wiley & Sons.
Liu, X., Zhou, W., Yang, L., Li, L., Zhang, Z., Ke, Y. & Chen, S. (2015). *J. Mater. Chem. A*, **3**, 8840–8846.
Lu, T., Zhuang, X., Li, Y. & Chen, S. (2004). *J. Am. Chem. Soc.* **126**, 4760–4761.
McWilliams, S. F., Bunting, P. C., Kathiresan, V., Mercado, B. Q., Hoffman, B. M., Long, J. R. & Holland, P. L. (2018). *Chem. Commun.* **54**, 13339–13342.
Miscione, G. P. & Bottoni, A. (2014). *Organometallics*, **33**, 4173–4182.
Öfele, K. (1969). *Angew. Chem. Int. Ed. Engl.* **8**, 916–917.
Pruppacher, H. R. & Klett, J. D. (1997). In *Microphysics of Clouds and Precipitation*. Dordrecht: Springer.
Raba, A., Cokoja, M., Ewald, S., Riener, K., Herdtweck, E., Pöthig, A., Herrmann, W. A. & Kühn, F. E. (2012). *Organometallics*, **31**, 2793–2800.
Regenauer, N. I., Wadepohl, H. & Roşca, D.-A. (2022). *Inorg. Chem.* **61**, 7426–7435.
Riener, K., Haslinger, S., Raba, A., Högerl, M. P., Cokoja, M., Herrmann, W. A. & Kühn, F. E. (2014). *Chem. Rev.* **114**, 5215–5272.
Saouma, C. T., Moore, C. E., Rheingold, A. L. & Peters, J. C. (2011). *Inorg. Chem.* **50**, 11285–11287.
Schlachta, T. P., Anneser, M. R., Schlagintweit, J. F., Jakob, C. H. G., Hintermeier, C., Böth, A. D., Haslinger, S., Reich, R. M. & Kühn, F. E. (2021). *Chem. Commun.* **57**, 6644–6647.
Schlachta, T. P. & Kühn, F. E. (2023). *Chem. Soc. Rev.* **52**, 2238–2277.
Schlachta, T. P., Zámbó, G. G., Sauer, M. J., Rüter, I. & Kühn, F. E. (2024). Submitted.
Sear, R. P. (2014). *CrystEngComm*, **16**, 6506–6522.
Sheldrick, G. M. (2015*a*). *Acta Cryst.* A**71**, 3–8.
Sheldrick, G. M. (2015*b*). *Acta Cryst.* C**71**, 3–8.
Spek, A. L. (2020). *Acta Cryst.* E**76**, 1–11.
Spentzos, A. Z., Gau, M. R., Carroll, P. J. & Tomson, N. C. (2020). *Chem. Commun.* **56**, 9675–9678.
Suess, D. L. M. & Peters, J. C. (2013). *J. Am. Chem. Soc.* **135**, 4938–4941.
Sunada, Y., Imaoka, T. & Nagashima, H. (2013). *Organometallics*, **32**, 2112–2120.
Takeshita, T., Sato, K. & Nakajima, Y. (2018). *Dalton Trans.* **47**, 17004–17010.
Walter, P., Welcomme, E., Hallégot, P., Zaluzec, N. J., Deeb, C., Castaing, J., Veyssière, P., Bréniaux, R., Lévêque, J.-L. & Tsoucaris, G. (2006). *Nano Lett.* **6**, 2215–2219.

supporting information

Acta Cryst. (2024). C**80** [https://doi.org/10.1107/S2053229624007058]

Formation of a diiron–(μ-η^1:η^1-CN) complex from acetonitrile solution

Tim P. Schlachta, Michael J. Sauer, Leon F. Richter and Fritz E. Kühn

Computing details

μ-Cyanido-κ^2C:N-bis[(acetonitrile-κN)[3,3′-bis(pyridin-2-yl)-1,1′-(methylidene)bis(benzimidazol-2-ylidene)]iron(II) tris(hexafluorophosphate),

Crystal data

$[Fe_2(CN)(C_2D_3N)_2(C_{25}H_{18}N_6)_2](PF_6)_3$
M_r = 1465.67
Monoclinic, *C*2/*c*
Hall symbol: -C 2yc
a = 25.562 (2) Å
b = 17.0373 (15) Å
c = 14.8998 (12) Å
β = 112.112 (3)°
V = 6011.8 (9) Å^3
Z = 4
F(000) = 2944
D_x = 1.613 Mg m^{-3}
Mo *K*α radiation, λ = 0.71073 Å
Cell parameters from 9628 reflections
θ = 2.4–26.4°
μ = 0.67 mm^{-1}
T = 100 K
Block, orange
0.13 × 0.05 × 0.04 mm

Data collection

Bruker D8 Venture diffractometer
Radiation source: TXS rotating anode
Helios optic monochromator
Detector resolution: 16 pixels mm^{-1}
phi– and ω–rotation scans
Absorption correction: multi-scan (SADABS; Bruker, 2016)
T_{min} = 0.708, T_{max} = 0.745
89835 measured reflections
5310 independent reflections
4621 reflections with $I > 2\sigma(I)$
R_{int} = 0.051
θ_{max} = 25.0°, θ_{min} = 1.8°
h = −30→30
k = −20→20
l = −17→17

Refinement

Refinement on F^2
Least-squares matrix: full
$R[F^2 > 2\sigma(F^2)]$ = 0.031
$wR(F^2)$ = 0.083
S = 1.11
5310 reflections
461 parameters
9 restraints
Primary atom site location: iterative
Secondary atom site location: difference Fourier map
Hydrogen site location: inferred from neighbouring sites
H-atom parameters constrained
$w = 1/[\sigma^2(F_o^2) + (0.0401P)^2 + 7.8548P]$ where $P = (F_o^2 + 2F_c^2)/3$
$(\Delta/\sigma)_{max}$ = 0.001
$\Delta\rho_{max}$ = 0.43 e Å^{-3}
$\Delta\rho_{min}$ = −0.27 e Å^{-3}

Special details

Experimental. Diffractometer operator Michael J. Sauer scanspeed 8 s per frame dx 52 mm 2745 frames measured in 9 data sets phi-scans with delta_phi = 0.5 omega-scans with delta_omega = 0.5 shutterless mode

Geometry. All esds (except the esd in the dihedral angle between two l.s. planes) are estimated using the full covariance matrix. The cell esds are taken into account individually in the estimation of esds in distances, angles and torsion angles; correlations between esds in cell parameters are only used when they are defined by crystal symmetry. An approximate (isotropic) treatment of cell esds is used for estimating esds involving l.s. planes.

Refinement. Refinement on F^2 for ALL reflections except those flagged by the user for potential systematic errors. Weighted R-factors wR and all goodnesses of fit S are based on F^2, conventional R-factors R are based on F, with F set to zero for negative F^2. The observed criterion of $F^2 > 2\text{sigma}(F^2)$ is used only for calculating -R-factor-obs etc. and is not relevant to the choice of reflections for refinement. R-factors based on F^2 are statistically about twice as large as those based on F, and R-factors based on ALL data will be even larger.

Fractional atomic coordinates and isotropic or equivalent isotropic displacement parameters (Å²)

	x	*y*	*z*	U_{iso}*/U_{eq}	Occ. (<1)
C2	0.51681 (9)	0.54639 (12)	0.40847 (15)	0.0230 (4)	
C1	0.48971 (8)	0.67342 (11)	0.41355 (14)	0.0191 (4)	
C3	0.52280 (10)	0.46741 (12)	0.39071 (16)	0.0285 (5)	
H3	0.493545	0.439133	0.342543	0.034*	
C4	0.57347 (10)	0.43178 (13)	0.44656 (16)	0.0325 (5)	
H4	0.578761	0.377839	0.436170	0.039*	
C5	0.61662 (10)	0.47228 (13)	0.51698 (16)	0.0309 (5)	
H5	0.650564	0.445503	0.553634	0.037*	
C6	0.61117 (9)	0.55136 (12)	0.53500 (15)	0.0262 (5)	
H6	0.640536	0.579456	0.583194	0.031*	
C7	0.56099 (9)	0.58683 (11)	0.47936 (14)	0.0210 (4)	
C8	0.41982 (8)	0.60040 (12)	0.29429 (14)	0.0216 (4)	
C9	0.39400 (9)	0.53318 (13)	0.24422 (16)	0.0278 (5)	
H9	0.412663	0.483855	0.258325	0.033*	
C10	0.34073 (10)	0.53986 (13)	0.17372 (16)	0.0316 (5)	
H10	0.322298	0.495149	0.137462	0.038*	
C11	0.31423 (9)	0.61226 (14)	0.15608 (17)	0.0315 (5)	
H11	0.277284	0.617889	0.108242	0.038*	
C12	0.34259 (9)	0.67626 (13)	0.20945 (15)	0.0269 (5)	
H12	0.324037	0.725698	0.197740	0.032*	
C13	0.57511 (9)	0.72591 (11)	0.54465 (15)	0.0237 (4)	
H13A	0.615637	0.718645	0.556805	0.028*	
H13B	0.570386	0.721898	0.607461	0.028*	
C14	0.50573 (8)	0.82068 (11)	0.43583 (14)	0.0185 (4)	
C15	0.55845 (8)	0.93306 (11)	0.47385 (14)	0.0194 (4)	
C16	0.58037 (8)	1.00883 (12)	0.48412 (15)	0.0220 (4)	
H16	0.558874	1.051346	0.447128	0.026*	
C17	0.63487 (9)	1.01944 (12)	0.55065 (15)	0.0251 (5)	
H17	0.651077	1.070411	0.559010	0.030*	
C18	0.66666 (9)	0.95765 (13)	0.60568 (16)	0.0261 (5)	
H18	0.703851	0.967543	0.650754	0.031*	
C19	0.64519 (9)	0.88182 (12)	0.59610 (15)	0.0241 (4)	
H19	0.666647	0.839438	0.633500	0.029*	

C20	0.59074 (8)	0.87146 (11)	0.52896 (14)	0.0205 (4)	
C21	0.45748 (8)	0.92713 (11)	0.34057 (14)	0.0191 (4)	
C22	0.44959 (9)	1.00394 (12)	0.30793 (15)	0.0229 (4)	
H22	0.477790	1.042564	0.336464	0.027*	
C23	0.39996 (9)	1.02300 (13)	0.23321 (16)	0.0276 (5)	
H23	0.393359	1.075350	0.209642	0.033*	
C24	0.35964 (9)	0.96551 (13)	0.19246 (16)	0.0277 (5)	
H24	0.325140	0.977582	0.140730	0.033*	
C25	0.37087 (9)	0.89035 (13)	0.22888 (14)	0.0240 (4)	
H25	0.343196	0.850972	0.200839	0.029*	
C26	0.37547 (9)	0.76394 (12)	0.48363 (15)	0.0223 (4)	
C27	0.33930 (9)	0.76348 (14)	0.53938 (16)	0.0314 (5)	
H27A	0.362703	0.760303	0.608611	0.047*	
H27B	0.313983	0.718030	0.520553	0.047*	
H27C	0.316874	0.811809	0.526464	0.047*	
N1	0.47349 (7)	0.60167 (9)	0.36928 (12)	0.0211 (4)	
N2	0.54219 (7)	0.66444 (9)	0.47956 (12)	0.0192 (3)	
N3	0.39514 (7)	0.67189 (10)	0.27707 (12)	0.0215 (4)	
N4	0.50588 (7)	0.89954 (9)	0.41663 (11)	0.0184 (3)	
N5	0.55693 (7)	0.80364 (9)	0.50275 (12)	0.0190 (3)	
N6	0.41879 (7)	0.86973 (10)	0.30185 (12)	0.0196 (4)	
N7	0.40318 (7)	0.76333 (10)	0.43942 (12)	0.0201 (4)	
N8	0.4815 (13)	0.7578 (5)	0.271 (3)	0.012 (3)	0.5
C28	0.5088 (17)	0.7573 (7)	0.226 (4)	0.015 (3)	0.5
F1	0.28817 (5)	0.30065 (8)	0.33162 (9)	0.0332 (3)	
F2	0.26765 (5)	0.36583 (8)	0.11822 (9)	0.0329 (3)	
F3	0.27050 (6)	0.41972 (7)	0.25915 (9)	0.0354 (3)	
F4	0.34412 (5)	0.34831 (8)	0.25648 (10)	0.0355 (3)	
F5	0.28548 (6)	0.24662 (7)	0.19108 (10)	0.0389 (3)	
F6	0.21189 (5)	0.31830 (9)	0.19278 (9)	0.0368 (3)	
P1	0.27795 (2)	0.33301 (3)	0.22461 (4)	0.02314 (14)	
Fe1	0.44743 (2)	0.75968 (2)	0.35901 (2)	0.01691 (9)	
P2	0.5028 (4)	0.77084 (6)	0.7390 (5)	0.0259 (9)	0.5
F7	0.4679 (2)	0.8423 (3)	0.6742 (5)	0.0414 (12)	0.5
F8	0.5148 (2)	0.8219 (3)	0.8346 (4)	0.0494 (13)	0.5
F9	0.53865 (16)	0.70063 (18)	0.8030 (3)	0.0597 (10)	0.5
F10	0.49183 (12)	0.72121 (15)	0.6430 (2)	0.0357 (6)	0.5
F11	0.44684 (14)	0.7360 (3)	0.7446 (2)	0.0606 (10)	0.5
F12	0.55908 (11)	0.80528 (18)	0.7315 (2)	0.0400 (7)	0.5

Atomic displacement parameters (Å²)

	U^{11}	U^{22}	U^{33}	U^{12}	U^{13}	U^{23}
C2	0.0285 (11)	0.0170 (10)	0.0230 (10)	−0.0014 (8)	0.0092 (9)	0.0028 (8)
C1	0.0226 (10)	0.0165 (10)	0.0206 (10)	−0.0039 (8)	0.0108 (8)	−0.0002 (8)
C3	0.0381 (13)	0.0164 (10)	0.0273 (11)	−0.0043 (9)	0.0081 (10)	−0.0004 (9)
C4	0.0450 (14)	0.0148 (10)	0.0332 (12)	0.0031 (9)	0.0094 (11)	0.0013 (9)
C5	0.0382 (13)	0.0181 (11)	0.0321 (12)	0.0059 (9)	0.0083 (10)	0.0048 (9)

C6	0.0309 (12)	0.0184 (11)	0.0265 (11)	0.0012 (9)	0.0076 (9)	0.0013 (8)
C7	0.0282 (11)	0.0143 (10)	0.0223 (10)	−0.0009 (8)	0.0116 (9)	0.0008 (8)
C8	0.0232 (10)	0.0202 (10)	0.0211 (10)	−0.0057 (8)	0.0081 (8)	0.0016 (8)
C9	0.0330 (12)	0.0195 (11)	0.0301 (12)	−0.0061 (9)	0.0109 (10)	−0.0012 (9)
C10	0.0347 (13)	0.0269 (12)	0.0312 (12)	−0.0130 (10)	0.0101 (10)	−0.0056 (9)
C11	0.0232 (11)	0.0333 (13)	0.0322 (12)	−0.0068 (9)	0.0040 (10)	−0.0026 (10)
C12	0.0229 (11)	0.0254 (11)	0.0305 (12)	−0.0027 (9)	0.0078 (9)	−0.0013 (9)
C13	0.0249 (11)	0.0147 (10)	0.0256 (11)	0.0021 (8)	0.0029 (9)	−0.0021 (8)
C14	0.0227 (10)	0.0145 (9)	0.0211 (10)	0.0015 (8)	0.0113 (8)	−0.0013 (8)
C15	0.0181 (10)	0.0193 (10)	0.0216 (10)	−0.0020 (8)	0.0084 (8)	−0.0047 (8)
C16	0.0257 (11)	0.0167 (10)	0.0256 (11)	−0.0003 (8)	0.0120 (9)	−0.0016 (8)
C17	0.0262 (11)	0.0193 (10)	0.0322 (12)	−0.0069 (8)	0.0136 (9)	−0.0070 (9)
C18	0.0196 (10)	0.0255 (11)	0.0308 (12)	−0.0030 (9)	0.0068 (9)	−0.0073 (9)
C19	0.0225 (10)	0.0194 (10)	0.0280 (11)	0.0019 (8)	0.0067 (9)	−0.0039 (8)
C20	0.0215 (10)	0.0168 (10)	0.0242 (10)	−0.0017 (8)	0.0099 (8)	−0.0043 (8)
C21	0.0200 (10)	0.0188 (10)	0.0205 (10)	0.0001 (8)	0.0101 (8)	−0.0008 (8)
C22	0.0248 (11)	0.0201 (10)	0.0252 (11)	−0.0009 (8)	0.0111 (9)	0.0005 (8)
C23	0.0308 (12)	0.0227 (11)	0.0303 (12)	0.0031 (9)	0.0125 (10)	0.0069 (9)
C24	0.0258 (11)	0.0290 (12)	0.0255 (11)	0.0025 (9)	0.0064 (9)	0.0064 (9)
C25	0.0207 (10)	0.0265 (11)	0.0232 (11)	−0.0012 (8)	0.0064 (9)	0.0001 (8)
C26	0.0209 (10)	0.0209 (10)	0.0218 (10)	0.0018 (8)	0.0043 (9)	0.0032 (8)
C27	0.0251 (11)	0.0418 (14)	0.0298 (12)	0.0049 (10)	0.0134 (10)	0.0073 (10)
N1	0.0242 (9)	0.0144 (8)	0.0234 (9)	−0.0031 (7)	0.0075 (7)	0.0000 (7)
N2	0.0207 (8)	0.0151 (8)	0.0201 (8)	−0.0002 (7)	0.0057 (7)	−0.0004 (6)
N3	0.0213 (9)	0.0200 (9)	0.0235 (9)	−0.0039 (7)	0.0087 (7)	−0.0012 (7)
N4	0.0194 (8)	0.0139 (8)	0.0216 (8)	−0.0003 (6)	0.0074 (7)	−0.0014 (7)
N5	0.0190 (8)	0.0153 (8)	0.0208 (8)	−0.0009 (7)	0.0053 (7)	−0.0027 (7)
N6	0.0192 (8)	0.0215 (9)	0.0197 (8)	−0.0001 (7)	0.0093 (7)	−0.0004 (7)
N7	0.0192 (8)	0.0181 (9)	0.0215 (9)	0.0005 (7)	0.0062 (7)	0.0012 (7)
N8	0.005 (9)	0.010 (3)	0.019 (2)	−0.001 (2)	0.003 (6)	0.000 (2)
C28	0.007 (9)	0.017 (4)	0.020 (3)	−0.001 (2)	0.004 (6)	0.000 (3)
F1	0.0328 (7)	0.0370 (7)	0.0277 (7)	0.0044 (6)	0.0092 (6)	0.0050 (6)
F2	0.0345 (7)	0.0352 (7)	0.0263 (7)	−0.0045 (6)	0.0085 (6)	0.0013 (5)
F3	0.0400 (8)	0.0265 (7)	0.0361 (7)	0.0070 (6)	0.0103 (6)	−0.0047 (6)
F4	0.0211 (6)	0.0412 (8)	0.0406 (8)	0.0003 (6)	0.0075 (6)	0.0046 (6)
F5	0.0550 (9)	0.0231 (7)	0.0479 (8)	0.0001 (6)	0.0298 (7)	−0.0045 (6)
F6	0.0217 (6)	0.0515 (9)	0.0340 (7)	−0.0047 (6)	0.0067 (6)	−0.0013 (6)
P1	0.0202 (3)	0.0226 (3)	0.0248 (3)	0.0012 (2)	0.0064 (2)	−0.0009 (2)
Fe1	0.01672 (15)	0.01537 (15)	0.01870 (15)	−0.00122 (11)	0.00674 (12)	−0.00098 (11)
P2	0.0273 (16)	0.0196 (4)	0.024 (3)	−0.0010 (8)	0.0018 (15)	0.0012 (7)
F7	0.047 (3)	0.026 (2)	0.042 (2)	0.0131 (17)	0.0055 (19)	0.0051 (16)
F8	0.056 (4)	0.053 (4)	0.031 (2)	0.004 (2)	0.007 (2)	−0.014 (2)
F9	0.063 (2)	0.0328 (18)	0.051 (2)	0.0012 (16)	−0.0151 (19)	0.0152 (16)
F10	0.0386 (15)	0.0250 (14)	0.0350 (15)	−0.0053 (11)	0.0042 (13)	−0.0107 (11)
F11	0.0415 (19)	0.099 (3)	0.0406 (19)	−0.029 (2)	0.0148 (16)	0.007 (2)
F12	0.0303 (15)	0.0353 (16)	0.0522 (18)	−0.0096 (12)	0.0130 (13)	−0.0107 (14)

Geometric parameters (Å, º)

C2—C3	1.391 (3)	C19—C20	1.386 (3)
C2—N1	1.403 (3)	C19—H19	0.9500
C2—C7	1.403 (3)	C20—N5	1.407 (3)
C1—N2	1.341 (3)	C21—N6	1.356 (3)
C1—N1	1.377 (3)	C21—C22	1.384 (3)
C3—C4	1.388 (3)	C21—N4	1.407 (3)
C3—H3	0.9500	C22—C23	1.375 (3)
C4—C5	1.386 (3)	C22—H22	0.9500
C4—H4	0.9500	C23—C24	1.385 (3)
C5—C6	1.391 (3)	C23—H23	0.9500
C5—H5	0.9500	C24—C25	1.378 (3)
C6—C7	1.377 (3)	C24—H24	0.9500
C6—H6	0.9500	C25—N6	1.343 (3)
C7—N2	1.407 (3)	C25—H25	0.9500
C8—N3	1.351 (3)	C26—N7	1.134 (3)
C8—C9	1.390 (3)	C26—C27	1.457 (3)
C8—N1	1.406 (3)	C27—H27A	0.9800
C9—C10	1.376 (3)	C27—H27B	0.9800
C9—H9	0.9500	C27—H27C	0.9800
C10—C11	1.384 (3)	Fe1—N3	2.0703 (16)
C10—H10	0.9500	Fe1—N6	2.0754 (17)
C11—C12	1.383 (3)	Fe1—N7	1.9336 (17)
C11—H11	0.9500	Fe1—C28^{i}	1.98 (5)
C12—N3	1.344 (3)	Fe1—N8	1.83 (4)
C12—H12	0.9500	Fe1—C1	1.824 (2)
C13—N2	1.460 (2)	Fe1—C14	1.824 (2)
C13—N5	1.463 (3)	N8—C28	1.128 (12)
C13—H13A	0.9900	F1—P1	1.6128 (13)
C13—H13B	0.9900	F2—P1	1.6063 (13)
C14—N5	1.345 (3)	F3—P1	1.5992 (13)
C14—N4	1.374 (2)	F4—P1	1.5968 (13)
C15—C16	1.392 (3)	F5—P1	1.5892 (13)
C15—C20	1.395 (3)	F6—P1	1.5924 (13)
C15—N4	1.413 (2)	P2—F11	1.580 (8)
C16—C17	1.384 (3)	P2—F9	1.588 (7)
C16—H16	0.9500	P2—F10	1.592 (6)
C17—C18	1.393 (3)	P2—F12	1.595 (8)
C17—H17	0.9500	P2—F8	1.598 (8)
C18—C19	1.390 (3)	P2—F7	1.600 (9)
C18—H18	0.9500		
C3—C2—N1	134.2 (2)	N6—C25—H25	118.2
C3—C2—C7	120.2 (2)	C24—C25—H25	118.2
N1—C2—C7	105.62 (17)	N7—C26—C27	178.9 (2)
N2—C1—N1	106.73 (17)	C26—C27—H27A	109.5
N2—C1—Fe1	132.87 (15)	C26—C27—H27B	109.5

N1—C1—Fe1	118.74 (14)	H27A—C27—H27B	109.5
C4—C3—C2	117.0 (2)	C26—C27—H27C	109.5
C4—C3—H3	121.5	H27A—C27—H27C	109.5
C2—C3—H3	121.5	H27B—C27—H27C	109.5
C5—C4—C3	122.2 (2)	C1—N1—C2	110.40 (16)
C5—C4—H4	118.9	C1—N1—C8	114.98 (16)
C3—C4—H4	118.9	C2—N1—C8	134.56 (17)
C4—C5—C6	121.3 (2)	C1—N2—C7	110.73 (16)
C4—C5—H5	119.4	C1—N2—C13	124.95 (16)
C6—C5—H5	119.4	C7—N2—C13	124.30 (16)
C7—C6—C5	116.6 (2)	C12—N3—C8	117.12 (17)
C7—C6—H6	121.7	C12—N3—Fe1	130.04 (14)
C5—C6—H6	121.7	C8—N3—Fe1	112.81 (13)
C6—C7—C2	122.75 (19)	C14—N4—C21	115.07 (16)
C6—C7—N2	130.72 (19)	C14—N4—C15	110.26 (16)
C2—C7—N2	106.52 (17)	C21—N4—C15	134.35 (17)
N3—C8—C9	123.18 (19)	C14—N5—C20	110.67 (16)
N3—C8—N1	112.53 (17)	C14—N5—C13	125.16 (16)
C9—C8—N1	124.28 (19)	C20—N5—C13	124.15 (16)
C10—C9—C8	118.4 (2)	C25—N6—C21	116.92 (17)
C10—C9—H9	120.8	C25—N6—Fe1	129.93 (14)
C8—C9—H9	120.8	C21—N6—Fe1	112.89 (13)
C9—C10—C11	119.4 (2)	C26—N7—Fe1	177.16 (17)
C9—C10—H10	120.3	F5—P1—F6	90.05 (8)
C11—C10—H10	120.3	F5—P1—F4	90.26 (8)
C12—C11—C10	118.7 (2)	F6—P1—F4	179.66 (8)
C12—C11—H11	120.6	F5—P1—F3	179.58 (8)
C10—C11—H11	120.6	F6—P1—F3	90.00 (8)
N3—C12—C11	123.2 (2)	F4—P1—F3	89.69 (7)
N3—C12—H12	118.4	F5—P1—F2	90.37 (7)
C11—C12—H12	118.4	F6—P1—F2	89.96 (7)
N2—C13—N5	110.78 (16)	F4—P1—F2	89.92 (7)
N2—C13—H13A	109.5	F3—P1—F2	90.05 (7)
N5—C13—H13A	109.5	F5—P1—F1	90.02 (7)
N2—C13—H13B	109.5	F6—P1—F1	89.98 (7)
N5—C13—H13B	109.5	F4—P1—F1	90.14 (7)
H13A—C13—H13B	108.1	F3—P1—F1	89.56 (7)
N5—C14—N4	106.69 (16)	F2—P1—F1	179.61 (8)
N5—C14—Fe1	132.79 (15)	C1—Fe1—C14	88.42 (9)
N4—C14—Fe1	119.49 (14)	C1—Fe1—N8	86.8 (7)
C16—C15—C20	120.54 (18)	C14—Fe1—N8	87.9 (9)
C16—C15—N4	133.87 (19)	C1—Fe1—N7	97.85 (8)
C20—C15—N4	105.58 (16)	C14—Fe1—N7	97.08 (8)
C17—C16—C15	117.04 (19)	N7—Fe1—N8	173.3 (10)
C17—C16—H16	121.5	Fe1^{i}—C28—N8	177 (4)
C15—C16—H16	121.5	Fe1—N8—C28	171.1 (7)
C16—C17—C18	121.99 (19)	C1—Fe1—N3	79.83 (8)
C16—C17—H17	119.0	N3—Fe1—C14	167.26 (8)

C18—C17—H17	119.0	N8—Fe1—N3	86.5 (7)
C19—C18—C17	121.46 (19)	N7—Fe1—N3	89.44 (7)
C19—C18—H18	119.3	C1—Fe1—N6	165.70 (8)
C17—C18—H18	119.3	C14—Fe1—N6	79.71 (7)
C20—C19—C18	116.29 (19)	N8—Fe1—N6	84.9 (5)
C20—C19—H19	121.9	N7—Fe1—N6	91.55 (7)
C18—C19—H19	121.9	N3—Fe1—N6	111.16 (7)
C19—C20—C15	122.68 (18)	F11—P2—F9	90.8 (3)
C19—C20—N5	130.53 (18)	F11—P2—F10	89.5 (4)
C15—C20—N5	106.79 (17)	F9—P2—F10	90.4 (2)
N6—C21—C22	123.10 (18)	F11—P2—F12	179.0 (4)
N6—C21—N4	112.40 (16)	F9—P2—F12	89.3 (5)
C22—C21—N4	124.50 (18)	F10—P2—F12	89.6 (3)
C23—C22—C21	118.4 (2)	F11—P2—F8	91.7 (3)
C23—C22—H22	120.8	F9—P2—F8	90.1 (5)
C21—C22—H22	120.8	F10—P2—F8	178.7 (5)
C22—C23—C24	119.7 (2)	F12—P2—F8	89.2 (4)
C22—C23—H23	120.2	F11—P2—F7	90.4 (5)
C24—C23—H23	120.2	F9—P2—F7	178.8 (6)
C25—C24—C23	118.3 (2)	F10—P2—F7	89.6 (5)
C25—C24—H24	120.8	F12—P2—F7	89.5 (3)
C23—C24—H24	120.8	F8—P2—F7	90.0 (2)
N6—C25—C24	123.6 (2)		

N1—C2—C3—C4	−179.7 (2)	C11—C12—N3—C8	−2.0 (3)
C7—C2—C3—C4	0.7 (3)	C11—C12—N3—Fe1	175.72 (16)
C2—C3—C4—C5	−0.1 (3)	C9—C8—N3—C12	1.5 (3)
C3—C4—C5—C6	−0.2 (4)	N1—C8—N3—C12	−177.18 (17)
C4—C5—C6—C7	−0.1 (3)	C9—C8—N3—Fe1	−176.56 (16)
C5—C6—C7—C2	0.7 (3)	N1—C8—N3—Fe1	4.7 (2)
C5—C6—C7—N2	179.7 (2)	N5—C14—N4—C21	173.84 (16)
C3—C2—C7—C6	−1.0 (3)	Fe1—C14—N4—C21	4.0 (2)
N1—C2—C7—C6	179.26 (19)	N5—C14—N4—C15	−0.6 (2)
C3—C2—C7—N2	179.78 (19)	Fe1—C14—N4—C15	−170.49 (13)
N1—C2—C7—N2	0.0 (2)	N6—C21—N4—C14	1.5 (2)
N3—C8—C9—C10	0.0 (3)	C22—C21—N4—C14	−178.39 (18)
N1—C8—C9—C10	178.6 (2)	N6—C21—N4—C15	174.24 (19)
C8—C9—C10—C11	−1.2 (3)	C22—C21—N4—C15	−5.6 (3)
C9—C10—C11—C12	0.8 (3)	C16—C15—N4—C14	−178.8 (2)
C10—C11—C12—N3	0.9 (3)	C20—C15—N4—C14	0.2 (2)
C20—C15—C16—C17	0.0 (3)	C16—C15—N4—C21	8.3 (4)
N4—C15—C16—C17	178.8 (2)	C20—C15—N4—C21	−172.8 (2)
C15—C16—C17—C18	−0.4 (3)	N4—C14—N5—C20	0.9 (2)
C16—C17—C18—C19	0.3 (3)	Fe1—C14—N5—C20	168.81 (15)
C17—C18—C19—C20	0.1 (3)	N4—C14—N5—C13	179.66 (17)
C18—C19—C20—C15	−0.4 (3)	Fe1—C14—N5—C13	−12.4 (3)
C18—C19—C20—N5	−179.3 (2)	C19—C20—N5—C14	178.2 (2)
C16—C15—C20—C19	0.4 (3)	C15—C20—N5—C14	−0.8 (2)

N4—C15—C20—C19	−178.70 (18)	C19—C20—N5—C13	−0.6 (3)
C16—C15—C20—N5	179.45 (17)	C15—C20—N5—C13	−179.59 (17)
N4—C15—C20—N5	0.4 (2)	N2—C13—N5—C14	23.9 (3)
N6—C21—C22—C23	0.5 (3)	N2—C13—N5—C20	−157.43 (17)
N4—C21—C22—C23	−179.58 (19)	C24—C25—N6—C21	0.1 (3)
C21—C22—C23—C24	−0.4 (3)	C24—C25—N6—Fe1	−173.70 (16)
C22—C23—C24—C25	0.1 (3)	C22—C21—N6—C25	−0.4 (3)
C23—C24—C25—N6	0.0 (3)	N4—C21—N6—C25	179.70 (16)
N2—C1—N1—C2	0.0 (2)	C22—C21—N6—Fe1	174.44 (15)
Fe1—C1—N1—C2	167.21 (14)	N4—C21—N6—Fe1	−5.4 (2)
N2—C1—N1—C8	−177.53 (16)	N2—C1—Fe1—C14	−2.1 (2)
Fe1—C1—N1—C8	−10.3 (2)	N1—C1—Fe1—C14	−165.21 (16)
C3—C2—N1—C1	−179.7 (2)	N2—C1—Fe1—N8	85.9 (9)
C7—C2—N1—C1	0.0 (2)	N1—C1—Fe1—N8	−77.2 (9)
C3—C2—N1—C8	−2.8 (4)	N2—C1—Fe1—N7	−99.0 (2)
C7—C2—N1—C8	176.8 (2)	N1—C1—Fe1—N7	97.86 (15)
N3—C8—N1—C1	2.7 (2)	N2—C1—Fe1—N3	173.0 (2)
C9—C8—N1—C1	−175.96 (19)	N1—C1—Fe1—N3	9.85 (14)
N3—C8—N1—C2	−174.0 (2)	N2—C1—Fe1—N6	31.7 (4)
C9—C8—N1—C2	7.3 (4)	N1—C1—Fe1—N6	−131.5 (3)
N1—C1—N2—C7	0.0 (2)	N5—C14—Fe1—C1	−0.1 (2)
Fe1—C1—N2—C7	−164.60 (16)	N4—C14—Fe1—C1	166.63 (16)
N1—C1—N2—C13	−178.60 (17)	N5—C14—Fe1—N8	−86.9 (7)
Fe1—C1—N2—C13	16.8 (3)	N4—C14—Fe1—N8	79.8 (7)
C6—C7—N2—C1	−179.2 (2)	N5—C14—Fe1—N7	97.64 (19)
C2—C7—N2—C1	0.0 (2)	N4—C14—Fe1—N7	−95.65 (15)
C6—C7—N2—C13	−0.6 (3)	N5—C14—Fe1—N3	−22.7 (5)
C2—C7—N2—C13	178.58 (18)	N4—C14—Fe1—N3	144.0 (3)
N5—C13—N2—C1	−26.0 (3)	N5—C14—Fe1—N6	−172.1 (2)
N5—C13—N2—C7	155.62 (17)	N4—C14—Fe1—N6	−5.36 (14)

Symmetry code: (i) −*x*+1, *y*, −*z*+1/2.

Hydrogen-bond geometry (Å, º)

D—H···*A*	*D*—H	H···*A*	*D*···*A*	*D*—H···*A*
C6—H6···F3^{ii}	0.95	2.58	3.437 (3)	150
C6—H6···F4^{ii}	0.95	2.58	3.348 (3)	138
C13—H13*A*···F1^{ii}	0.99	2.42	3.312 (2)	150
C13—H13*B*···F10	0.99	2.26	3.006 (4)	131
C13—H13*B*···F11^{iii}	0.99	2.42	3.396 (4)	170
C13—H13*B*···F12	0.99	2.43	3.257 (4)	140
C16—H16···F7^{iv}	0.95	2.47	3.366 (6)	158
C19—H19···F1^{ii}	0.95	2.62	3.513 (2)	158
C22—H22···F7^{iv}	0.95	2.44	3.310 (7)	152
C22—H22···F8^{v}	0.95	2.50	3.352 (7)	150
C25—H25···F6^{vi}	0.95	2.55	3.034 (2)	112
C27—H27*A*···F9^{iii}	0.98	2.57	3.299 (4)	131

C27—H27*A*···F11	0.98	2.37	3.286 (4)	155
C27—H27*A*···F12^{iii}	0.98	2.58	3.497 (4)	155
C27—H27*B*···F2^{vii}	0.98	2.62	3.348 (3)	131
C27—H27*C*···F2^{vi}	0.98	2.58	3.346 (3)	135

Symmetry codes: (ii) −*x*+1, −*y*+1, −*z*+1; (iii) −*x*+1, *y*, −*z*+3/2; (iv) −*x*+1, −*y*+2, −*z*+1; (v) *x*, −*y*+2, *z*−1/2; (vi) −*x*+1/2, *y*+1/2, −*z*+1/2; (vii) *x*, −*y*+1, *z*+1/2.